Thermodynamics applied to deformation structures

HANS RAMBERG

Ramberg, H., 1988 12 30: Thermodynamics applied to deformation structures, *Bulletin of the Geological Institutions of the University of Uppsala*, N.S., Vol. 14, pp. 1–12 Uppsala. ISSN 0302-2749.

In the geological sciences thermodynamics is chiefly used in the treatment of mineral assemblages. However, the laws of thermodynamics are not limited to chemical phase problems but are equally well applicable to mechanical phenomena such as the deformation of rocks due to deviatoric stress and/or the body force of gravity.

The failure of many attempts to explain preferred mineral orientation in strained rocks in terms of classical equilibrium thermodynamics illustrates the need to apply "Non-equilibrium thermodynamics" or the "Thermodynamics of Processes" in which "Extreme Rate of Entropy Production" or "Extreme Rate of Energy Dissipation" are governing principles.

Combined with the laws of classical mechanics, thermodynamical concepts control the evolution of deformation structures ranging in scale from crenulation cleavage, through folds and boudinage, to diapirs and orogenic nappes. Buckle folding and calculations of the velocity of the advance of thrust sheets are presented as examples.

H. Ramberg, Institute of Geology, University of Uppsala, Box 555, S-751 22 Uppsala, Sweden. *Received 17th June, 1987; revision received 3rd March, 1988.*

Introduction

In view of the successful application of thermodynamics to mineral assemblages in metamorphic rocks in the last 30 years or so, it is encouraging to find that deformation structures in plastico-viscous rocks may also successfully be treated by thermodynamic methods. Admittedly, the few published treatments of even rather simple deformation structures such as preferred mineral orientation in strained rocks have not been especially successful, e.g. MacDonald (1957), Kamb (1959, 1961), Verhoogen (1951).

However, I believe the reason for this lack of success is the use of equilibrium thermodynamics rather than open system thermodynamics or non equilibrium thermodynamics which is required for the study of solids yielding under stress. Crystals exposed to deviatoric stress do not represent equilibrium. As long as the deviatoric stress acts, the situation is intrinsically unstable and, for rocks exhibiting no defined yield point, an equilibrium state will not be reached as long as the stress remains deviatoric. Diffusion and various kinds of chemical processes make regional metamorphic rocks yield and flow at stresses much below the short-term yield strength as measured by the rock mechanicists in the laboratory.

Accordingly, classical equilibrium thermodynamics cannot be expected to yield useful information or profound understanding when it comes to structures developed under deviatoric stress. The theories of "non equilibrium thermodynamics", "open system thermodynamics" or the "thermodynamics of processes" must be applied.

These three terms are synonyms for the kind of thermodynamics which is applicable to systems not in equilibrium, see e.g. Onsager (1931), Prigogine (1947, 1967), Prigogine & Stegers (1984) and Gyarmati (1970).

The chief rule for the control of the evolution of systems not in equilibrium – for example mechanically stressed systems – is that the path of evolution is determined by prevalence of those processes which dissipate energy with extremum rate. Depending upon whether the velocities of the various processes or the forces are varied during the operation of seeking the extremum, the latter is either a maximum or a minimum.

For viscous processes, production of entropy is equal to dissipation of energy divided by the instantaneous temperature. Hence the criterium for the prevalent process: "extremum rate of dissipation of energy" is equivalent to "extremum rate of production of entropy". Onsager (1931) uses "extremum (minimum) dissipation of energy" as the controlling principle, while Prigogine (1947) applies "extremum (minimum) production of entropy" as the controlling factor. What is stated above means that the structures which develop in non equilibrium systems are controlled by the details of the processes which take place.

This condition clashes with a basic premise of equilibrium thermodynamics, viz. the premise that the equilibrium situation as manifested by the minerals that develop, their exact chemical composition etc. – is completely independent of the ways and means by which equilibrium is reached.

As examples on how structures in deformed rocks are controlled by the criteria of non equilibirum thermodynamics, of open system thermodynamics or of the equivalent thermodynamics of processes, we shall consider

(1) buckling of an embedded sheet of rock, and

(2) the gravitational spreading of a composite orogenic nappe.

Both systems have been treated in earlier publications (Buckling: Biot, 1961; Fletcher, 1977; Smith, 1975; Smoluchowski 1909; Ramberg 1962, 1981; Spreading: Price, 1973; Elliott, 1976; Ramberg, 1986) but not from the view point of non equilibrium thermodynamics.

Buckle folding of embedded layer

The model consists of a layer with high effective viscosity embedded between two half spaces of low viscosity (In practice the half spaces are layers with thicknesses exceeding the wavelength of the folds that form.)

Compression parallel to layering produces folds along the embedded layer. The problem is to find the preferred – or dominant – wavelength which tends to develop from a spectrum of statistical fluctuations of initial sinusoidal deflections with very small amplitudes. The mechanism which controls the initial wavelength of those deflections that survive and grow during evolution of the system is activated at the very beginning of the buckling process. When seeking the preferred wavelength it is therefore sufficient to consider infinitisimal motion and strain.

The problem is well suited to demonstrate that either maximum or minimum rate of energy dissipation or rate of entropy production can be used to find the "preferred path of evolution" of the system.

In systems of this kind the "preferred path of evolution" is manifested by a preferred – or dominant – wavelength of the folds which develop. To find the initial wavelength of the buckle folds which prevail during evolution of the system, the rate of growth of amplitude in most studies is calculated as a function of the wavelength of the corresponding fold and of the compressive force.

The preferred wavelength is found to coincide with the maximum rate of relative growth of amplitude if the compressive force is kept equal for the spectrum of wavelengths which may develop.

When the compressive force is kept equal and constant, and the amplitude/wavelength ratio is small, then maximum rate of amplitudinal growth means maximum rate of energy input due to the buckling force. This is so because maximum rate of relative growth of amplitude coincides with maximum rate of relative shortening of wavelength due to buckling. This will be demonstrated below.

If, on the other hand, the energy of evolution of the folds is based on equal rate of relative growth of amplitude while the compressive force is varied then the preferred wavelength coincides with minimum buckling force and with minimum rate of energy input.

To focus the discussion let us consider briefly the dynamic analysis of the model.

It was mentioned above that different methods have been used in the analysis of viscous buckling. A "thick-plate-bending method" similar to one often used in applied mechanics, is not the most exact one but it is simple and quite illuminating, demonstrating very well the essential points of the buckling phenomenon. For more exact analyses see Biot (1961), Fletcher (1977), Smith (1975), Ramberg (1970).

Restricted to small amplitude/wavelength ratios and Newtonian materials the compressive layer-parallel force needed to buckle the layer itself is calculated for different rates of compression and combined with the force needed to press the bends into the adjacent materials and there produce the so-called contact strain on either side of the layer.

In this way relationships are obtained between the rate of growth of amplitude or the rate of shortening of wavelength and the compressive stress parallel to the general trend of the buckling layer. See eqns (1 and 6). The general trend of the layer is the line joining the inflection points of the row of buckles. Eqns. (1) is an acceptable approximation at $\phi < 1$.

(1) $$\sigma_b/\eta_2=(4/(Rm\phi)-\phi/(3Rm)+(2/Rm+2\phi/3)\ (\phi/2+\phi^2/(6Rm)\ )\ /\ (1+\phi/Rm\ +\phi^2/3)\ )v/y$$

$Rm=\eta_1/\eta_2$, $\phi=2\pi H/\lambda$, λ is wavelength and η_1/η_2 is the viscosity ratio. In this equation (a rearrangement of eqn (63) in Ramberg, 1962) the amplitudinal velocity divided by the instantaneous amplitude – v/y – is termed the "relative amplitudinal growth rate" and σ_b/η_1 – the buckling stress divided by the viscosity of the layer – is referred to as the "normalized buckling stress". The quantity in the parenthesis in front of "v/y" corresponds in magnitude to the normalized buckling stress needed to generate a relative amplitudinal growth rate of unit magnitude. It is practical to assign a special name to this quantity: "Specific normalized buckling stress". This indicates the character of the quantity which measures the normalized stress specifically needed to make the amplitude grow at a rate of unit relative velocity. The thus defined "*S*pecific *no*rmalized *b*uckling *s*tress" will be referred to by the letters *Snobs*, and eqn (1) can be identified by a much shortened expression:

(2) $\sigma_b/\eta_1 = Snobs\ v/y$

We see that *Snobs* contains only two variables, the viscosity ratio $Rm=\eta_1/\eta_2$, and the ratio H/λ which occurs in $\phi=2\pi H/\lambda$.

Both variables are dimensionless and so is *Snobs* itself. When *Snobs* is plotted as a function of the wavelength/thickness ratio at selected values of η_1/η_2 we find that *Snobs* goes through a minimum at a λ/H ratio which depends upon the magnitude of η_1/η_2. This is presented in Fig 1.

If the rate of relative amplitudinal growth is kept constant for the spectrum of wavelengths which may occur, then eqn (2) shows that the normalized buckling stress goes through a numerical minimum at the same wavelength/thickness ratio as does *Snobs*.

For a given buckling layer with uniform thickness, the buckling force (=stress multiplied by the thickness of the layer times its length parallel to the fold axis) assumes minimum value at the same λ/H ratio as does the stress. This is the wavelength/thickness ratio for which the buckling process meets least viscous resistance and accordingly by Gauss' Principle of Least Constraint, is the initial wavelength of those viable buckles which will survive and grow; i.e. the buckles with the dominant wavelength.

With the non equilibrium thermodynamics of Onsager and Prigogine in mind it is interesting to see if the rate of dissipation of energy (cf. Onsager, 1931) and/or the rate of production of entropy (cf. Prigogine, 1947) also assume minimal values at the same wavelength which minimizes the buckling force and the viscous resistance.

The rate of input of energy per wavelength is the buckling force multiplied by the rate of buckle-shortening per wavelength.

(Buckle-shortening defines the shortening which is due solely to the periodic sidewise deflection of the layer. Shortening by homogeneous pure shear is not considered in the energy calculation). To evaluate the energy input it is necessary to find how the rate of relative shortening of wavelength is related to the rate of relative amplitudinal growth.

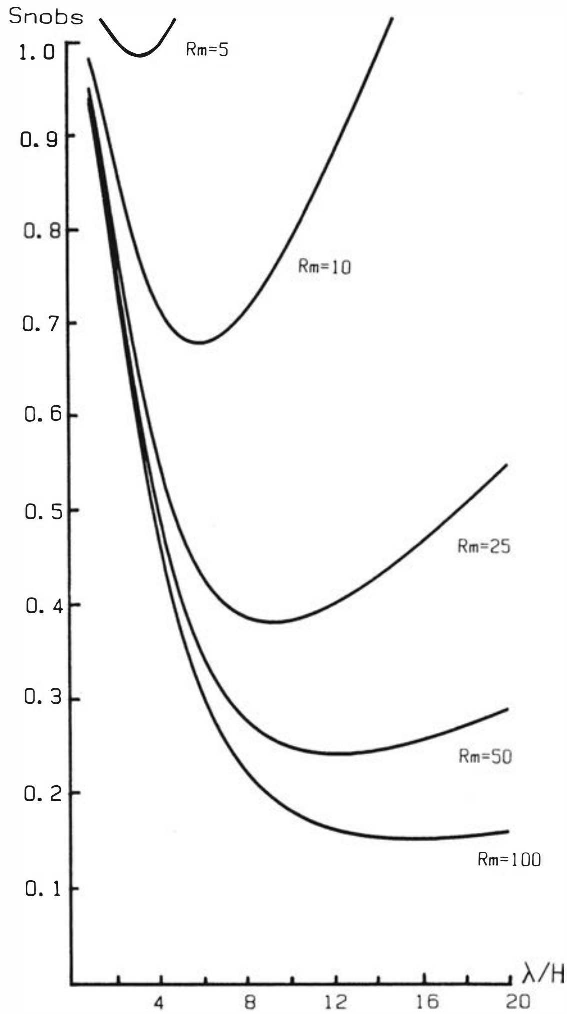

Fig. 1. *Snobs*=specific normalized buckling stress plotted as a function of wavelength/thickness ratio. Minimum on *Snobs* curve defines the preferred wavelength/thickness ratio. $Rm=\eta_1/\eta_2$.

For sinusoidal buckles with small ampliude/wavelength ratio the rate of shortening is related to the rate of growth of amplitude by the approximation

(3) $\dot{\lambda} = -2\pi^2 yv/\lambda$

This equation is readily modified to give the relation between the rate of relative shortening of wavelength and rate of relative amplitudinal growth:

(4) $\dot{\lambda}/\lambda = -2\pi^2 (y/\lambda)^2 v/y$

(5) $v/y = -1/(2\pi^2(y/\lambda)^2)\ \dot{\lambda}/\lambda$

 Bull. Geol. Inst. Univ. Uppsala, N.S. 14 (1988)

If v/y in equation (1) is replaced by above expression then an equation is obtained relating the normalized buckling stress to the rate of relative shortening of wavelength, $\dot{\lambda}/\lambda$, eqn (6).

(6) $\sigma_b/\eta_1 = ((4/(Rm\phi) - \phi/(3Rm) + (2/Rm + 2\phi/3) (\phi/2 + \phi^2/(6Rm)) /(1 + \phi/Rm + \phi^2/3)) / (-2\pi^2 (y/\lambda)^2))\dot{\lambda}/\lambda,$

or:

(7) $\sigma_b/\eta_1 = -Snobs/(2\pi^2 (y/\lambda)^2)\dot{\lambda}/\lambda$

The proportionallity factor between σ_b/η_1 and $\dot{\lambda}/\lambda$ is *Snobs* multiplied by the quantity $-1/(2\pi^2 (y/\lambda)^2)$.

It is to be expected that, statistically, the amplitudes of deflections caused by buckling are proportional to the wavelengths of the corresponding buckles. To the extent that this is true, the quantity

$-1/(2\pi^2 (y/\lambda^2)$

is constant for all waves in the spectrum of deflections. As shown by eqn (7), when the rate of relative shortening is constant then the buckling stress – and by implication the buckling force – are minimized at the same λ/H ratio which minimizes *Snobs*. At constant rate of relative shortening, the rate of energy input is minimized when the stress is minimized. We conclude from what has been stated above that for constant relative velocity – constant rate of relative amplitudinal growth, or constant rate of wavelength shortening as the case may be – then energy input rate, energy dissipation rate and entropy production rate are all minimized at the wavelength/thickness ratio of the dominant wave. Some examples are presented in Fig. 1.

After these comments on the energy of buckling constrained by constant rate of relative amplitudinal growth, and constant rate of relative shortening of wavelength while the normalized buckling stress is varied, we shall continue to discuss the energetics of buckling, but now constrained by equal buckling stress for all wavelengths while the rate of relative amplitudinal growth and the rate of relative shortening of wavelength are permitted to vary.

For this purpose it is practical to invert eqn (2):

(8) $v/y = 1/Snobs\ \sigma_b/\eta_1 = Ramp\ \sigma_b/\eta_1$

In this form of the relationship, the normalized buckling stress is the independent variable and the relative amplitudinal growth rate is the dependent variable.

The inverse of *Snobs* is termed *Ramp* and defines the value which the rate of *r*elative *amp*litudinal

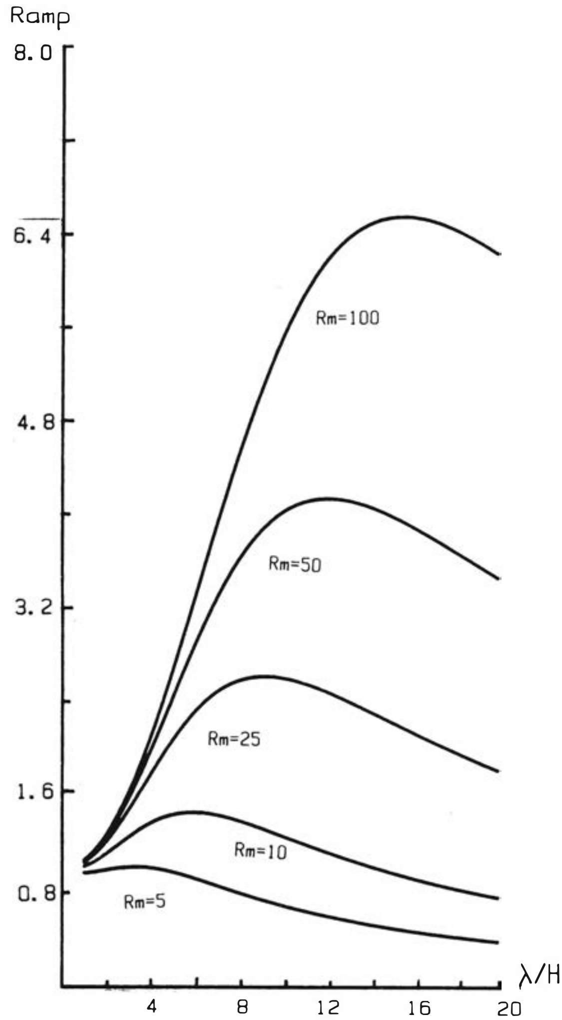

Fig. 2. Ramp=relative amplification plotted as a function of wavelength/thickness ratio. Maximum on *Ramp* curve defines the preferred wavelength/thickness ratio. *Rm*= η_1/η_2.

growth assumes when the value of the normalized buckling stress is equal to unity.

Ramp may be referred to as the "*r*elative *amp*lification" because it amplifies the relative amplitudinal growth rate in proportion to the normalized buckling stress.

Since *Snobs* as a function of λ/H goes through a numerical minimum at a wavelength/thickness ratio which depends upon the ratio η_1/η_2 it is evident that *Ramp*, being the inverse of *Snobs*, must go through a maximum at the same wavelength/thickness ratio at corresponding visosity ratio. This is demonstrated in Fig. 2.

Provided the normalized buckling stress is kept constant and equal for the whole spectrum of potential wavelengths of the buckles, then v/y and *Ramp* are linearly related and it follows that the relative amplitudinal growth rate goes through maximal value at the same λ/H ratio as that which minimized the buckling stress in the previous model with constant amplitudinal growth rate. On account of the established linear relation between relative amplitudinal growth rate and rate of relative shortening of wavelength, it follows that the maximum rate of input of driving energy coincides with the preferred wavelength. In other words, if the buckling stress is kept constant and the rate of relative growth of amplitude is allowed to vary, then it is maximum rate of energy dissipation, and maximum rate of entropy production, which are the criteria that determine the "preferred path of evolution".

Spreading of an orogenic nappe

The two-dimensional nappe consists of two layers, a bottom layer (1) with thickness H_1, constant viscosity η_1 and density ϱ_1, and an upper layer (2) whose relevant properties are H_2, η_2 and ϱ_2.

The motion in the system is approximated by two polynomial stream functions:

$$(9)\quad \psi_1=-(ay_1^2+by_1^3+dy_1^4+ey_1^5+fy_1^6)\,x_1+(cy_1^2+5/3dy_1^3+10/3ey_1^4+14/3fy_1^5)\,x_1^3-(ey_1^2+7/3fy_1^3)\,x_1^5$$

valid for layer (1), and:

$$(10)\quad \psi_2=(a_{21}+a_{22}y_2+a_{23}y_2^2+a_{24}y_2^3+a_{25}y_2^4+a_{26}y_2^5)\,x_2+(a_{41}+a_{42}y_2-a_{25}y_2^2-a_{61}y_2^2-5/3a_{26}y_2^3-5/3a_{62}y_2^3)\,x_2^3+(a_{61}+a_{62}y_2)x_2^5$$

valid for layer (2).

The equations are selected from the stream function solutions given in Ramberg (1986). For these two functions to yield information on velocity, strain, stress etc. the coefficients must be determined. Determination of the coefficients is partly done by applying the boundary constraint of continuous normal and shear stress as well as continuous velocity at the contact between the two layers. The lack of shear at the free top surface of layer (2) is also used for coefficient determination. This operation leads to all coefficients in stream function two, i.e. a_{21} to a_{62} in eqn (10) and c, d, e and f in eqn (9), being related to a and b in stream function (9). For details see Ramberg (1986).

It is for the final determination of a and b that the principles of non equilibrium thermodynamics are useful. Non equilibrium thermodynamics requires that the rate of dissipation of potential energy due to viscous strain shall assume an extreme value. (For the case in question the extremum is a maximum, in accord with the condition that the force is the same for all possible processes that constitute the yield, while the velocities are variable, see earlier discussion in the section on buckling).

To apply the requirement of extremum dissipation or extremum entropy production, formulas for the energies are needed.

The instantaneous rate of change of strain energy is obtained by integrating the specific strain energy rate, $\dot{e}_x + \dot{e}_{xy}$ (= the energy rate per volume):

$$(11)\quad \dot{e}_x = 4\eta_i\dot{\varepsilon}_x^2 = 4\eta_i(\partial u/\partial x)^2 = 4\eta_i(-\partial^2\psi/\partial x\partial y)^2,$$

and

$$(12)\quad \dot{e}_{xy} = \eta^1\dot{\gamma}_{xy}^2 = \eta^1\,(\partial u/\partial y + \partial v/\partial x)^2 = (\partial^2\psi/\partial x^2 - \partial^2\psi/\partial y^2)^2$$

and the specific potential energy rate:

$$(13)\quad \dot{e}_{pot} = \varrho_i\,gv = \varrho_i g\,\partial\psi/\partial x$$

over a cross section slice of unit thickness parallel to the plane x, y through the model. η_1 and ϱ_1 are used for the portion of the slice that cuts layer (1) and η_2 and ϱ_2 for the portion that cuts through layer (2). Here u and v are velocity components in horizontal and vertical directions respectively; $\dot{\gamma}_{xy}$ is shear strain rate, $\dot{\varepsilon}_x$ is rate of longitudinal strain in direction x and g is acceleration of gravity. The integration leads to the two energy equations (14) and (15)

$$(14)\quad \dot{E}_{\varepsilon\gamma} = \eta_2\,(A_{\varepsilon\gamma}a^2H_2^4 + B_{\varepsilon\gamma}b^2H_2^6 + C_{\varepsilon\gamma}\,abH_2^5)$$

for the strain energy rate, and

$$(15)\quad \dot{E}_{pot} = \varrho_2 g\,(A_{pot}aH_2^4 + B_{pot}bH_2^5),$$

referring to the potential energy rate.

Both equations are valid for the whole cross section slice of unit thickness.

The factors $A_{\varepsilon\gamma}$, $B_{\varepsilon\gamma}$, $C_{\varepsilon\gamma}$, A_{pot} and B_{pot} in front of the coefficients a and b are now known, but much too lengthy to present in full here: the interested reader is referred to the author's original publication op cit. 1986. It is worth mentioning, though, that the factors in question are functions of but three variables, viz. the thicknesses of the two layers and the length of the cross section.

(In eqns (14) and (15) only the properties of layer

(2) seem to occur; but that is because thickness, density and viscosity of layer (1) are "hidden" in the factors $A_{\varepsilon\gamma}$, $B_{\varepsilon\gamma}$, $C_{\varepsilon\gamma}$, A_{pot} and B_{pot}).

In equations (14) and (15) all is known except the two coefficients a and b which in fact control the remaining coefficients in both stream functions. A determination of a and b accordingly makes the stream functions numerically applicable to the model.

To obtain numerical values for a and b by the method of maximizing the dissipation rate we make use of the Lagrange Multiplier. To this end a new function, F, is formed:

$$(16) \quad \dot{F} = \dot{E}_{pot} + \lambda(\dot{E}_{pot} + \dot{E}_{\varepsilon\gamma})$$

and the partial derivatives of $\dot{F}$ with respect to a, b and λ are put equal to zero. Note that $E_{pot} + E_{\varepsilon\gamma} = 0$ is the side condition stating that strain energy rate at all time is balanced by the rate of decline of potential energy. λ in the above equation is called the Lagrange Multiplier. For explanation of the Lagrange Multiplier method see Protter and Morrey (1964).

From the set of three homogeneous equations developed when the partial derivatives are equated to zero, it is possible to eliminate λ and determine the coefficients a and b. The thus found values for a and b are inserted in the functions that relate the remaining stream function coefficients to a and b, a_{21}, a_{22}. . . a_{61}, a_{62} and c, d, e, f as functions of a and b are now inserted in stream functions (9) and (10) from which the instantaneous velocity field follows by differentiation:

$$u = -\partial\psi/\partial y \text{ and } v = \partial\psi/\partial x$$

These instantaneous velocity fields may then be multiplied by a reasonable time step to give the initial displacement field.

Numerical examples are discussed in the section below.

Models with aspect ratio R_2=2

Fig. 3*A* shows an initial undeformed profile with a set of vertical passive strain markers, valid for models *B*, *C* and *D*. H_2=5000 m and H_1=50 m. H_1 is exaggerated by a factor 10 in *A*. Density of both layers, $\varrho_1 = \varrho_2$ = 2.8g/cm^3 and viscosity of layer 2, η_2, equals 10^{22} poise while the viscosity of the basal layer varies: $\eta_1 = 10^{22}$ poise in *B*, 10^{17} poise in *C* and 10^{16} poise in *D*. *B*, *C* and *D* show the deformed shape after $5 \cdot 10^5$ years had the initial instantaneous velocity been constant during this length of time.

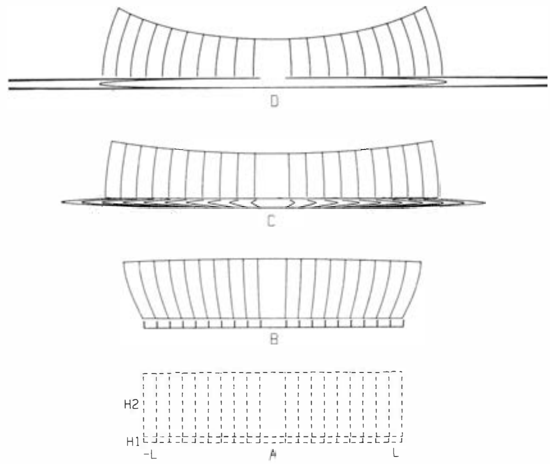

Fig. 3. Gravitational spreading of double layer viscous structure with basal layer 1, 50 m thick, density 2.8 g/cm^3 and viscosity 10^{22} poise in *B*, 10^{17} poise in *C* and 10^{16} poise in *D*; and an upper layer 2, 5000 m thick, density 2.8g/cm^3 and viscosity 10^{22} poise. Aspect ratio $R_2 = L/H_2 = 2$. *A* shows initial profile with passive markers, H_1 of basal layer exaggerated by factor 40. *B*, *C* and *D* show deformed profiles had initial velocity remained constant during 5 10^5 years. As velocity is actually not constant the deformations visualize variation of initial velocity at the boundary and at the markers rather than the final shape, see text and Tables 1 and 2. The velocity of extrusion of layer 1 in D is so large that the front would be far outside the limit of the illustration.

The velocity is of course not constant for which reason the deformed shape is to be regarded as a geometric visualization of the varying initial velocity at the boundary rather than a final shape. (One may wonder what is the source of the viscosity value 10^{22} poise which we use so frequently in the models? The source is Haskel (1935); 10^{22} poise is the classical value for the average viscosity of the crust and the upper part of the mantle treated as a unit and calculated by Haskel based on data from the rate of postglacial uplift in Scandinavia).

It is interesting to consider how the deformation – or more exact: the initial velocity field – varies with changing viscosity of the basal layer.

If there is no differencce between the viscosity of the two layers, then the deformation in the basal layer is chiefly simple shear caused by drag from the superincumbent mass whose lateral spreading increases upward. In model *B* there is very little vertical squeezing of layer 1 and its viscosity is too high to permit horizontal extrusion. Along its base, layer 2 encounters great resistance due to the combination: high viscosity and small thickness of layer 1. The mean pressure in the central part of layer 2 is therefore relatively high as in fact indicated by the

Table 1. U_1 and V_1 are horizontal and vertical velocities at the contact between the two layers at the front face; U_2 and V_2 are horizontal and vertical velocities at the top of the front face of layer 2. The last value of U_1 for each model is the maximal extrusion velocity of layer 1 at the viscosity in question.
Ufree is the average velocity of the front face and Vfree the average velocity of decline of the top surface of layer 2 if there were free slip at the base.
All velocities are in cm/year. See Tables 2, 3, 4 and 5. η_1 is in poise. Column "η" gives the exponent in the expression for the viscosity.

H_2=5000 m, H_1=50 m, $\eta_2=10^{22}$ poise, $\varrho_1=\varrho_2=2.8$g/cm_3

R_2=2, Ufree=.532192, Vfree=−.260963

η_1	U_1	U_2	V_1	V_2
22	.005246	.303135	−.000018	−.129849
21	.051646	.336734	−.000160	−.143911
20	.301692	.438062	−.000696	−.183188
19	.516955	.487478	−.000971	−.188127
18	.556004	.492318	−.001177	−.182853
17	.571188	.471632	−.003998	−.143409
17	1.269168	See Table 2		

R_2=5, Ufree=1.330481, Vfree=−.260963

η_1	U_1	U_2	V_1	V_2
22	.005853	.336135	−.000019	−.129954
21	.058645	.393264	−.000177	−.156038
20	.415098	.663204	−.000868	−.234619
19	1.075757	1.139646	−.001236	−.257297
18	1.311789	1.315541	−.001273	−.255344
17	1.342923	1.336334	−.001321	−.246014
16	1.354070	1.323144	−.004846	−.173244
16	3.688546			

R_2=20, Ufree=5.321925, Vfree=−.266096

η_1	U_1	U_2	V_1	V_2
22	.003570	.183400	−.000004	−.026791
21	.039037	.236291	−.000043	−.037432
20	.399076	.605228	−.000431	−.115289
19	1.672415	1.767629	−.001161	−.240920
18	4.078730	4.103834	−.001330	−.268224
17	5.200633	5.203771	−.001336	−.268588
16	5.357413	5.357175	−.001325	−.262666
15	5.375086	5.370487	−.002536	−.211332
15	7.521821	See Table 3		

R_2=100, Ufree=26.609625, Vfree=−.26609625

η_1	U_1	U_2	V_1	V_2
22	.000812	.041224	0	−.001250
21	.009167	0.54804	0	−.001817
20	.125064	.187395	−.00003	−.008025
19	1.214855	1.276036	−.000289	−.059854
18	5.501544	5.531198	−.001012	−.203781
17	15.633015	15.642454	−.001320	−.265235
16	24.839256	24.840800	−.001342	−.269725
15	26.654741	26.654867	−.001333	−.267422
14	26.854354	26.853979	−.001469	−.244853
13	26.865604	26.864924	−.002065	−.222380
13	30.954932	See Table 4		

R_2=200, Ufree=53.219255, Vfree=−.2660925

η_1	U_1	U_2	V_1	V_2
22	.000408	.020695	0	−.000314
21	.004609	.027545	0	−.000457
20	.063783	.095530	0	−.002054
19	.704641	.739809	−.000086	−.017852
18	4.952857	4.978176	−.000561	−.112965
17	17.174310	17.184053	−.001206	−.242250
16	40.942609	40.945132	−.001338	−.268913
15	52.030121	52.030422	−.001341	−.269424
14	53.574745	53.574728	−.001327	−.263519
13	53.735459	53.735006	−.002520	−.212086
13	74.725421	See Table 5		

gentle convex curvature of the top surface of the model. (Due to the great vertical exaggeration of layer 1 in drawing *B* (here about 20 times) it is hard to recognize the gentle tilt of the passive markers which indicate the magnitude of the small shear strain in layer 1. In models with greater shear strain along the base the tilt of the markes is very pronounced, see Fig. 4).

The relatively low viscosity of layer 1 in model *C* permits a considerable amount of vertical squeezing by the weight of the overburden, and in-spite of its small thickness, layer 1 is extruded quite rapidly. Details of the velocity distribution are recorded in Tables 1 and 2. The horizontal motion during extrusion generates shear stress at the contact to layer 2 which accordingly becomes exposed to horizontal tensile stress, increasing in intensity from zero at the front face(s) to maximal value in the center of the symmetrical body. As the vertical normal stress component is compressive throughout layer 2 the result is a deviatoric stress which causes horizontal tensile strain that gives rise to maximal stretching in the center and a concave upper surface of the model. The extrusion of a relatively "soft" basal stratum and its effect on a more competent overburden is enhanched if the viscosity of the basal stratum is decreased. This is demonstrated in model *D* where the viscosity of layer 1 is no more than 10^{16}

Table 2. Horizontal, U_1 and U_2, and vertical, V_1 and V_2, velocity in cm/year at different levels at the front face of layer 1 and 2 in models with aspect ratio 2 and different viscosity of the basal layer. Ni gives height of level in each layer, expressed in parts of the full heights H_1 and H_2. Note that U_1 is maximum close to the middle level in layer 1, and that U_2 increases toward the base, assuming maximum value at the contact between the two layers. The latter condition is evidence of drag from the extruding mass of the basal layer.

H_2=5000m, H_1=50m, $\eta_2=10^{22}$ poise, $\varrho_1=\varrho_2$=2.8g/cm$_3$

$R_2=2$, $\eta_1=10^{16}$ poise

U_1	U_2	V_1	V_2	Ni
.623642	.371312	−.081194	−.023246	1
9.338533	.418161	−.078932	−.036160	.9
16.102923	.460207	−.072769	−.046851	.8
20.916812	.497448	−.063678	−.055560	.7
23.780200	.529887	−.052635	−.062527	.6
24.693087	.557522	−.040616	−.067993	.5
23.655473	.580353	−.028595	−.072196	.4
20.667357	.598381	−.017547	−.075377	.3
15.728740	.611605	−.008449	−.077778	.2
8.839621	.620025	−.002275	−.079636	.1
0.000000	.623642	−0.000000	−.081194	0

$\eta^1=10^{17}$ poise, $R_2=2$

U_1	U_2	V_1	V_2	Ni
.571188	.471632	−.003998	−.143409	1
.861490	.490161	−.003759	−.132281	.9
1.074587	.506786	−.003382	−.120275	.8
1.210480	.521506	−.002904	−.107485	.7
1.269168	.534320	−.002365	−.094006	.6
1.250652	.545229	−.001803	−.079934	.5
1.154931	.554233	−.001257	−.065363	.4
.982005	.561331	−.000765	−.050389	.3
.731875	.566523	−.000366	−.035106	.2
.404540	.569809	−.000098	−.019611	.1
0.000000	.571188	−0.000000	−.003998	0

poise, in other words, even less than that of rock salt which under natural conditions appears to exhibit an effective viscosity around 10^{17} poise. In model *D* the maximal rate of extrusion is no less than 24.69 cm/year as recorded in Table 2.

Models with aspect ratio R_2=5

Models R_2=5;A, B, C whose right half profiles are shown in Fig. 4 start out with initial aspect ratio R_2=5 (stippled outline). H_2=5000 m, H_1=50 m, $\eta_2=10^{22}$ poise and $\varrho_1=\varrho_2$=2.8g/cm^3. Viscosity η_1 is 10^{22} in *A*, 10^{17} in *B* and 10^{16} for *C*, all in poise.

The thin basal layer is not plotted in *A*. In *B* and *C* the thickness of layer 1 is greatly exaggerated to show the strain of the initally straight vertical passive markers.

The R_2=5 models show many similarities with the R_2=2 models displayed in Fig. 3. The convex shape of the upper surface of model R_2=5,*A* whose viscosity η_1 is high (10^{22} poise), the central stretching of layer 2 in models with softer basal layer and the concave shape of the surface of the latter models are qualitative repetitions of features exhibited by the R_2=2 models in Fig. 3. There are, however, interesting quantitative differences. One of these is the relationship between the aspect ratio – or rather the length of the horizontal dimension since the height is the same for the models – and the value of the viscosity of layer 1 at which extrusion occurs. In models with aspect ratio R_2=2 extrusion occurred when the viscosity η_1 is as high as 10^{17} poise whereas in models with R_2=5 extrusion does not take place unless the viscosity of the basal layer is 10^{16} poise or less. This well displayed effect in the two sets of models proves to be generally valid: the greater the aspect ratio – for models with the same thicknesses, H_1 and H_2, – the less viscous must the basal layer be for extrusion to occur. This conclusion is not only intuitively reasonable but also well documented by the relationships found in models with aspect ratio 20, 100 and 200. Some relevant information is recorded in Tables 1, 3, 4 and 5.

Models with aspect ratio R_2=20

Also in these models H_2=5000m, H_1=50m, $\eta_2=10^{22}$ poise and $\varrho_1=\varrho_2$=2.8 g/cm^3

Fig 5 shows deformed shapes after $5\cdot10^5$ years assuming steady velocity equal to the initial velocity. In *B* the viscosity of the not shown basal layer is 10^{22} poise. In *A* $\eta_1=10^{15}$ poise. The stippled outline in *A* is the initial profile of layer 2, also valid for model *B*. The passively deformed, initially straight and vertical markers in layer 1 are seen in *A* where the thickness of the layer is greatly exaggerated. In *A* a very faint concave curvature of the top surface is possibly noticable, in accord with the horizontal tensile stress created in layer 2 by drag from the extruding basal stratum.

In the R_2=20 models the length is 100 km and it is only reasonable that the basal layer has to be rather mobile for extrusion to occur. The calculation puts 10^{15} poise as the maximum limit for the viscosity which permits extrusion of layer 1. This is visualized in Fig. 5, numerical detailes are reported in Tables 1 and 3.

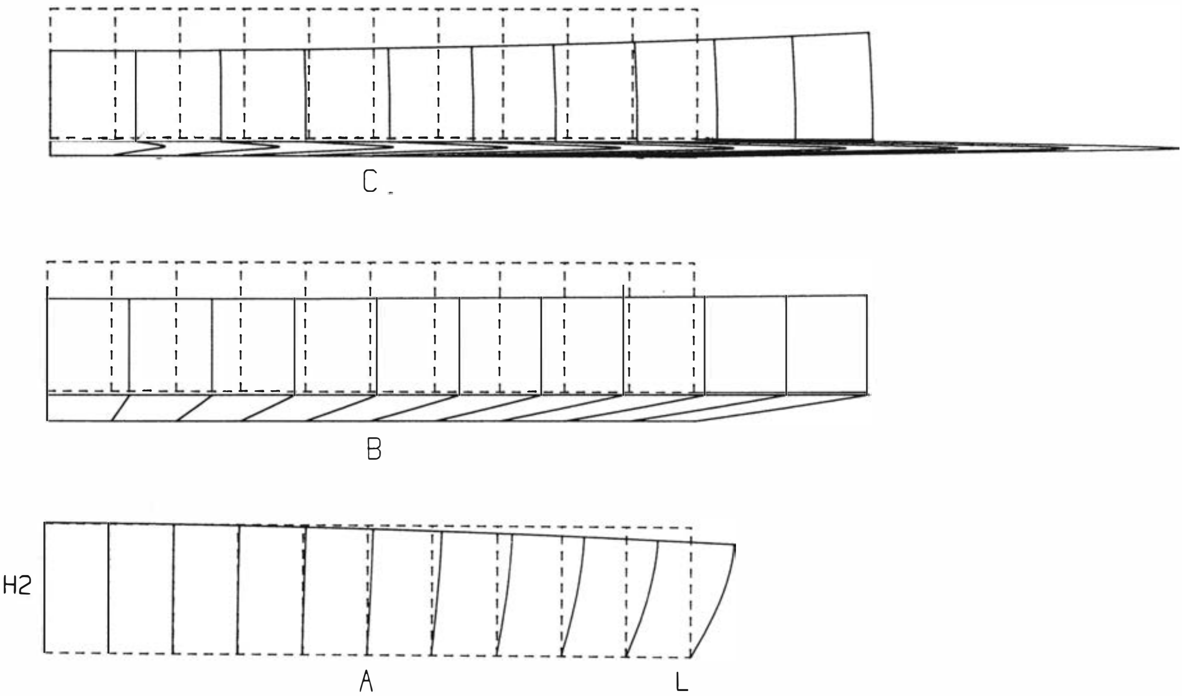

Fig. 4. Right half of spreading double layer viscous structure. Stippled outline shows initial profile containing passive markers; aspect ratio $R_2=L/H_2=5$. Layer 1 not shown in *A*; in *B* and *C* thickness H_1 greatly exaggerated. Solid profile and markers define deformation after 5 10^5 years had the initial velocity been constant during that time. Thickness H_2=5000m, H_1=50m, density of both layers 2.8g/cm^3, viscosity of layer 2 is 10^{22} poise in all models, viscosity of layer 1 is 10^{22} poise in *A*, 10^{17} poise in *B* and 10^{16} poise in *C*. See text and Tables 1 and 2.

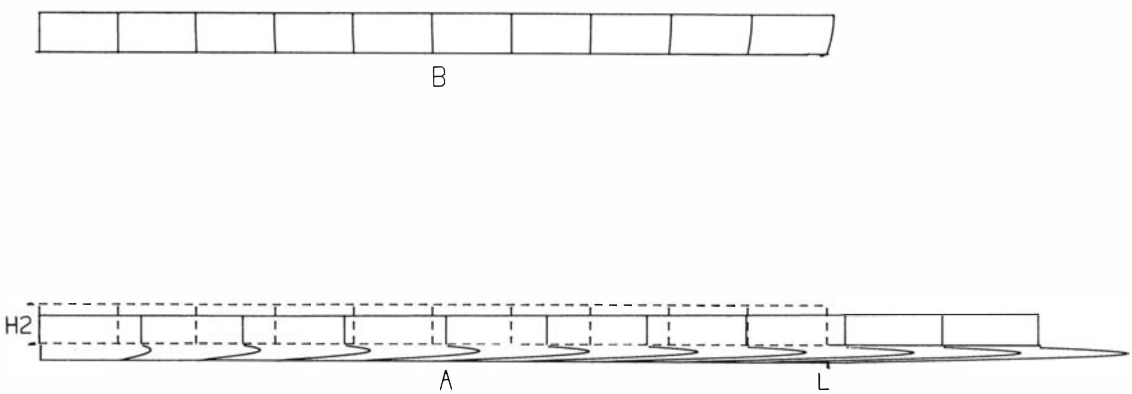

Fig. 5. Spreading double layer viscous structure with aspect ratio $R_2=L/H_2=20$, H_2=5000m, H_1=50m (not shown in *B* and greatly exaggerated in *A*), viscosity of layer 2 is 10^{22} poise in both models, viscosity of layer 1 is 10^{22} in *B* and 10^{15} in *A*. Density is 2.8g/cm^3 in both layers.
Initial profile with passive markers stippled in *A*. Solid outline and markers define deformation after 5. 10^5 years had the initial velocity been unchanged. See text and Table 3.

Table 3. Horizontal, U_1 and U_2, and vertical, V_1 and V_2, velocity in cm/year at differen levels at the front face of layer 1 and 2 in model with aspect ratio R_2=20. Ni gives hight of level in each layer, expressed in parts of the full heights H_1 and H_2. Note that U_1 assumes maximum at level between Ni=.6 and .7 in layer 1, and that U_2 shows a small increases toward the base, assuming maximum value at the contact between the two layers. The latter condition is evidence of drag from the extruding mass of the basal layer.

H_2=5000m, H_1=50 m, R_2=20, $\eta_2=10^{22}$ poise, $\eta_1=10^{15}$ poise $\varrho_1=\varrho_2=2.8$g/cm^3.

U_1	U_2	V_1	V_2	Ni
5.375085	5.370486	−.002535	−.211332	1
6.448688	5.371345	−.002295	−.190465	.9
7.164267	5.372115	−.002004	−.169594	.8
7.521820	5.372796	−.001680	−.148720	.7
7.521349	5.373389	−.001342	−.127842	.6
7.162853	5.373893	−.001006	−.106962	.5
6.446332	5.374308	−.000692	−.086080	.4
5.371786	5.374635	−.000416	−.065195	.3
3.939215	5.374874	−.000196	−.044309	.2
2.148620	5.375024	−.000052	−.023423	.1
0.000000	5.375085	−0.000000	−.002535	0

Table 4. Horizontal, U_1 and U_2, and vertical, V_1 and V_2, velocity in cm/year at differen level at the front face of layer 1 and 2 in model with aspect ratio R_2=100. Ni gives height of level in each layer, expressed in parts of the full heights H_1 and H_2. Note that U_1 assumes maximum at level between Ni=.7 and .8 in layer 1, and that U_2 shows a small increases toward the base, assuming maximum value at the contact between the two layers. The latter condition is evidence of drag from the extruding mass of the basal layer.

H_2=5000m, H_1=50m, R_2=100, $\eta_1=5\cdot10^{13}$ poise, $\eta_2=10^{22}$ poise $\varrho_1=\varrho_2=2.8$g/cm^3.

U_1	U_2	V_1	V_2	Ni
26.865664	26.864924	−.002065	−.222380	1
29.385798	26.865063	−.001829	−.200349	.9
30.748887	26.865187	−.001569	−.178318	.8
30.954932	26.865297	−.001295	−.156287	.7
30.003932	26.865392	−.001021	−.134255	.6
27.895888	26.865474	−.000757	−.112224	.5
24.630799	26.865540	−.000516	−.090192	.4
20.208666	26.865593	−.000307	−.068161	.3
14.629488	26.865631	−.000144	−.046129	.2
7.893266	26.865655	−.000038	−.024097	.1
0.000000	26.865664	−0.000000	−.002065	0

Models with aspect ratio R_2=100 and 200

With aspect ratio 100 or more, 5000 m thick structures will extend horizontally 500 km or more; models with R_2=200 will initially extend 1000 km across the base.

Numerical models with dimensions of this order are believed to be informative as regard the motion of thrust sheets.

Obviously a plot of models with R_2=100 or 200 on a page of the actual size is hardly meaningful – the plot will simply be a line across the page no more than a couple of milimeters thick. Relevant results from the computation are therefore only presented numerically, Tables 4 and 5.

Again the significant geometrical and mechanical properties are: H_2=5000 m, H_1=50 m, $\eta_2=10^{22}$ poise and $\varrho_1=\varrho_2=2.8$gm/cm^3. Tables 1, 4 and 5 display the velocities at selected values of η_1. As expected when $\eta_1=\eta_2$ then the velocity at corresponding points is less for model R_2=200 than for model R_2=100, and both structures are considerably less mobile than models R_2=2, R_2=5 and R_2=20 provided also the latter are compared under the condition $\eta_1=\eta_2$.

However, the most interesting and perhaps somewhat surprising result obtained is that models with large aspect ratios move faster than models with smaller aspect ratios if the viscosity of the basal stratum is less than certain limits, even if the high viscosity of layer 2 remains unchanged. The comparison is of course made among models whose viscosity of corresponding layers are the same. As an example, assume a basal layer whose effective viscosity compares with that often accepted for rock salt, say 10^{17} poise. Let the viscosity of layer 2 remain at the usual 10^{22} poise. Under these conditions

Table 5. Horizontal, U_1 and U_2, and vertical, V_1 and V_2, velocity in cm/year at differen levels at the front face of layer 1 and 2 in model with aspect ratio R_2=200. Ni gives height of level in each layer, expressed in parts of the full heights H_1 and H_2. Note that U_1 assumes maximum at level between Ni=.6 and .7 in layer 1, and that U_2 shows a small increases toward the base, assuming maximum value at the contact between the two layers. The latter condition is evidence of drag from the extruding mass of the basal layer.

H_2=5000m, H_1=50m, R_2=200, $\eta_1=10^{13}$ poise, $\eta_2=10^{22}$ poise, $\varrho_1=\varrho_2=2.8$g/cm^3

U_1	U_2	V_1	V_2	Ni
53.735459	53.735006	−.002520	−.212086	1
64.266456	53.735090	−.002280	−.191129	.9
71.263110	53.735166	−.001990	−.170173	.8
74.725421	53.735234	−.001668	−.149216	.7
74.653389	53.735292	−.001331	−.128260	.6
71.047014	53.735342	−.000998	−.107303	.5
63.906297	53.735383	−.000686	−.086347	.4
53.231237	53.735415	−.000412	−.065390	.3
39.021834	53.735439	−.000195	−.044433	.2
21.278088	53.735453	−.000052	−.023477	.1
0.000000	53.735459	−0.000000	−.002520	0

the data in Table 1 demonstrate that the rate of forward motion increases very markedly indeed, when the aspect ratio becomes large. Consider the top edge of the front face which moves with the horizontal velocity U_2=.472 for R_2=2, 1.336 for R_2=5, 5.203 for R_2=20, 15.642 for R_2=100 and not less than 17.184 for R_2=200, all in cm/year.

This obviousy too fast spreading will be moderated by higher effective viscosity of the real rocks, by rock members with finite strength in the heterogeneous natural structures, by less height of the natural profiles and by their gentler slope.

In accord with the large aspect ratios of the present models the critical viscosity for extrusion of layer 1 is small, viz. $5 \cdot 10^{13}$ poise for the models with aspect ratio 100, and 10^{13} poise for models with aspect ratio 200, Tables 4 and 5.

Strain in the basal layer

The large number of numerical tests performed on models similar to those described here have given interesting information on the behaviour of the basal layer in response to changing viscosity.

Let all parameters be constant except viscosity η_1 in a model with aspect ratio R_2=5, heights H_2=5000 m and H_1=50 m, viscosity $\eta_2=10^{22}$ poise and density $\varrho_1=\varrho_2$=2.8 g/cm^3.

The strain in the basal layer is visualized by deformation of the initially straight, vertical passive markers shown stippled in the initial profile of layer 1, see Fig. 6A where the thickness is exaggerated by a factor 40. As the viscosity of layer 1 diminishes from η_1=5 10^{16} to 9 10^{15} poise through steps $4 \cdot 10^{16}$, $3 \cdot 10^{16}$, $2 \cdot 10^{16}$, $1.5 \cdot 10^{16}$, 10^{16} to $9 \cdot 10^{15}$ poise the verti-

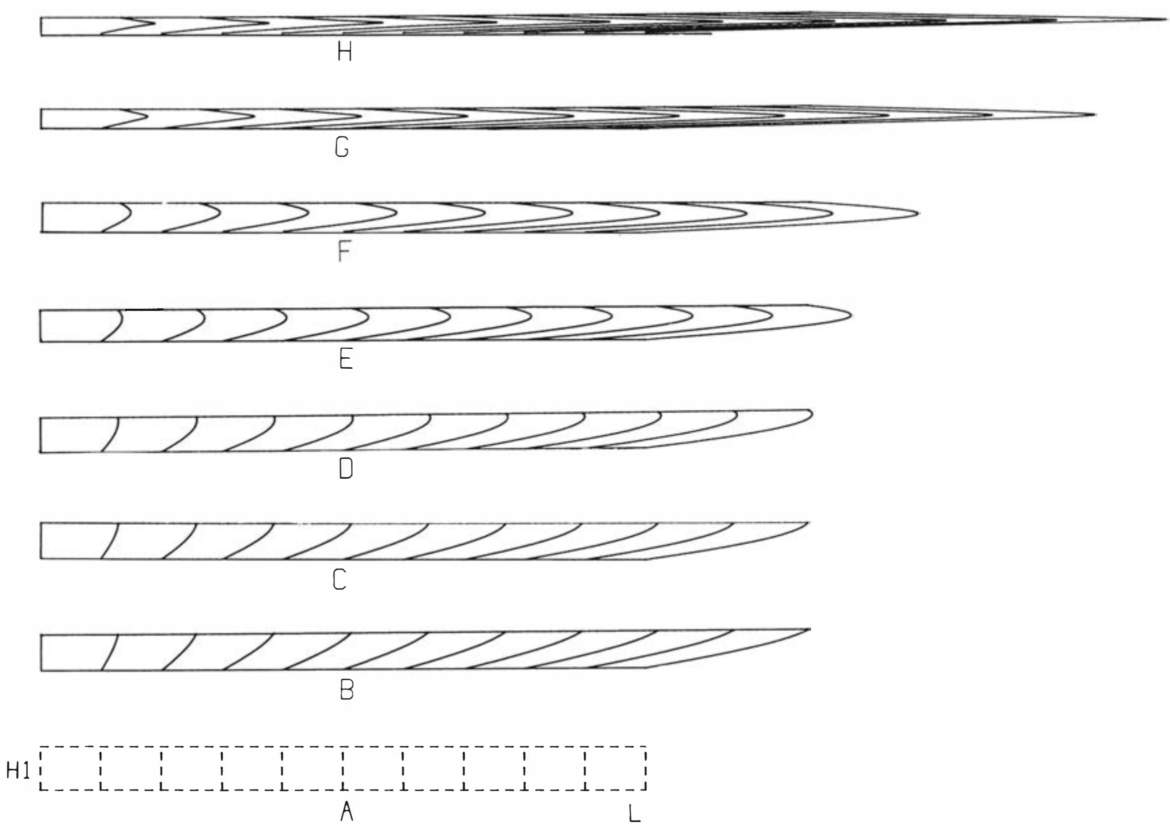

Fig. 6. Strain in layer 1 in spreading double layer viscous structure. Layer 2 not shown. H_2=5000m, H_1=50m, R_2=5, viscosity of layer 2 is 10^{22} poise and density of both layers 2.8g/cm^3. Viscosity of layer 1 is $5 \cdot 10^{16}$ in *B*, $4 \cdot 10^{16}$ in *C*, $3 \cdot 10^{16}$ in *D*, $2 \cdot 10^{16}$ in *E*, $1.5 \cdot 10^{16}$ in *F*, 10^{16} in *G* and $9 \cdot 10^{15}$ in *H*, all in poise. Initial profile and undeformed passive markers stippled in A where thickness H_1 is exaggerated by a factor 40. Profile of layer 1 and distorted markers would have been as shown for different viscosities in *B* to *H* had the initial velocity been unchanged during 5 10^5 years. The increasingly long extruded lobe in *D, E, F, G, H* visualizes the magnitude of the initial velocity of extrusion rather than the final shape of the extruded material.

cal squeezing and the rate of extrusion are intensified. If the viscosity of layer 1 is relatively high the passive markers are chiefly affected by the horizontal motion of layer 2 which tilts the markers by displacing their top in the direction of motion. (At the same time the small vertical compression and horizontal extension of layer 1 give the markers a gentle curvature, the convex side facing down to the right; see Fig. 6, B and C).

If the viscosity of layer 1 is gradually decreased the intensified extrusion makes its effect on the strain in layer 1 more and more markedly as is visualized by the changing shape of the strain markers in Fig. 6. It is interesting to note how the level of maximum horizontal flow rate gradually moves concordant with the decrease of the viscosity η_1, from the contact against layer 2 to the central level in layer 1, where maximum flow rate (due to maximum extensive strain rate) remains even if the viscosity is further decreased. (Fluid dynamicist readers will recognize that the type of flow developed in layer 1 is not unlike "Couette flow" which is characterized by slow non-inertial flow in the space between parallel plates, one of which moves with or against the fluid. Cole, 1962, p.86. The vertical compression which is necessary to drive the "fluid" flow in the present models is however not active in normal Couette flow, in which also the velocity of flow is constant along the channel.

The type of strain in layer 1 is essentially a combination of simple shear parallel to the layering and pure shear with axis of maximum extension parallel to the layering; that is, maximum extensive strain of the pure shear part coincides with the shear direction in the simple shear part. Within narrow contact zones along the base and along the contact with layer 2, the strain is chiefly simple shear; in a narrow zone along the level of maximum horizontal motion the strain is essentially pure shear. In the intervening space on either side of maximum extension pure and simple shear occur together, the relative partition of the two types changing gradually from simple shear along the contacts to pure shear within the zone of maximum horizontal flow rate.

The strain discussed here is associated with a pressure gradient pointing from the edges of layer 1 toward the center. The pressure gradient assumes maximum value at the edges and diminishes toward the center where it becomes zero. The horizontal flow in layer 1 increases in intensity from zero at the central cross section to maximal values at the two edges.

REFERENCES

Biot, M. A., 1961: Theory of folding of stratified viscoelastic media and its implication on tectonics and orogenesis. *Geol. Soc.Am. Bull. 72:* 1595.

Cole, G. H. A., 1962: *Fluid Dynamics,* Methuen et Co, London, 238 pp.

Elliott, D., 1976: The motion of thrust sheets, *J. Geophys., 81:* 949.

Fletcher, R. C., 1977: Folding of a single viscous layer, *Tectonophysics, 39:* 593.

Gyarmati, F., 1970: *Non-equilibrium thermodynamics,* Springer, Berlin, 184 pp.

Haskel, N.,A., 1935: The Motion of a Viscous Fluid under a Surface Load, *Physics, 6,* 265.

Jaeger, J. C., 1956: *Elasticity, Fracture and Flow,* Methuen, London, 152 pp.

Kamb, W.B., 1959: Theory of preferred crystal orientation developed under stress, *Jour. Geol., 67:* 153–170.

Kamb, W.B., 1961: The thermodynamic theory of nonhydrostatically stressed solids, *Jour. Geophys. Research, 66* (1): 259, 271.

MacDonald, G.J.F., 1957: Thermodynamics of solids under non-hydrostatic stress, with geological implications, *Amer. J. Sci., 255:* 266–281.

Onsager, L., 1931: Reciprocal Relations in Irreversible Processes, I and II, *Physical Review, 37,* 405–426; 38, 2265–2279.

Price, R. A., 1973: Large scale gravitational flow of supracrustal rocks. In K.A.deJong and R.Scholten: *Gravity and tectonics,* Wiley, New York.

Prigogine, I., 1947: *Etude thermodynamique des phenomenes irreversible* (thesis), Dunod, Paris.

Prigogine, I., 1967: *Introduction to themodynamics of irreversible processes,* 3rd ed. Wiley-Interscience, New York.

Prigogine, I. and Isabelle Stegers, 1984: *Order out of chaos,* Bantam Books, New York, 336 pp.

Protter, M. and C.B. Morrey, 1964: *Modern Mathematical Analysis.* Addison-Wesley, Reading, 790 pp.

Ramberg, H., 1962: Contact strain and folding instability of a multilayered body under compression, *Geol. Rundsch., 51*(2): 405–439.

Ramberg, H., 1970: Folding of laterally compressed multilayers in the field of gravity, 2, Numerical examples, *Phys. Earth Planet. Interiors, 4:* 83–120.

Ramberg, H., 1981: *Gravity, Deformation and the Earths Crust, 2nd Ed.* Academic Press, London, New York, Toronto, Sydney, 452 pp.

Ramberg, H., 1986: The stream function and Gauss principle of least constraint, two useful concepts for structural geology, *Tectonophysics, 131:* 205–246.

Smith, R. B., 1975: Unified theory of the onset of folding etc., *Geol., Soc., Amer., Bull., 86:* 1601.

Smoluchowski, M., 1909: Uber ein gewisses Stabilitatsproblem der elastizitatslehre etc., *Abhandl. Akad. Wiss., Krakau, Math., Kl 3.*

Van Nostrands Scientific Encyclopedia, 1958, 1839 pp.

Verhoogen, J., 1951: The chemical potential of a stressed solid Amer. *Geophys. Union Trans., 32:* 251.

Printed by Ekenäs Tryckeri Ab, Ekenäs, Finland December 30th, 1988